An Education Model of a Nano-Positioning System for Mechanical Engineers

Dong-Yeon Lee*, Dae-Gab Gweon
Department of Mechanical Engineering,
Korea Advanced Institute of Science and Technology (KAIST),
373-1 Guseong-Dong, Yuseong-Gu, Daejeon 305-701, Korea

The increasing use of nano-positioners in a wide variety of laboratory and industrial applications has created a need for nano-mechatronics education in all engineering disciplines. The subject of nano-mechatronics is broad and interdisciplinary. This article focuses on the way nano-mechatronics is taught in department of mechanical engineering at Korea Advanced Institute of Science and Technology (KAIST). As one model of nano-positioning systems, design and experimental methodology is presented in this article. For design phase, the stiffness and resonant frequencies are found analytically and verified by using a commercial finite element analysis program. Next, for experimental phase, various tests are performed to access the performances of the designed nano-positioner, for example, sine-tracking, multi-step response and travel-range check etc. Finally, the definition of "separation frequency" is described and some comments are discussed.

Key Words: Nano-positioning System, Education Model, Flexure-guide, Piezoelectric Actuator, Separation Frequency

1. Introduction

1.1 Motivation

The term "mechatronics" is of japanese origin and was introduced to qualify the dual alliance of electronics and computer technology to practical control applications in mechanical systems since 1970s. However, mechatronics educations have been concentrated on micrometer-accuracy level applications for example, industrial robot applications. Nowadays, focus is shifted into nanometer-accuracy level applications for example, atomic force microscopes (AFMs) which need very precise nano-positioning scanners. Since the invention of the AFMs in 1986 by physical scientists, many mechanical engineers have contributed to upgrade the design of the AFM by adopting nano-positioning systems which are comprised of the flexure-guide and the piezoelectric actuators. (Meek et al., 2003 ; Bojarski et al., 1995 ; Giurgiutiu et al., 2005 ; Tan et al., 1998 ; UME and Timmerman, 1995 ; Rizzoni and Keyhani, 1995 ; Acar and Parkin, 1996 ; Fraser et al., 1992 ; Ye et al., 2004 ; Chisholm, 1990)

As authors as know, there are few education courses of nano-positioning system in universities of Korea. Thus, there are lack of well-trained "nano-engineers" in industries. In this work, authors have developed an education model of a nano-positioning system for mechanical engineers at Korea Advanced Institute of Science and Technology (KAIST). The level of education is a graduate level. Hopely, this model would be a "role-model" of the nano-positioning training for practicing nano-engineers.

* Corresponding Author,
E-mail : ldymav@kaist.ac.kr
TEL : +82-42-869-8763; **FAX** : +82-42-869-8763
Department of Mechanical Engineering, Korea Advanced Institute of Science and Technology (KAIST), 373-1 Guseong-Dong, Yuseong-Gu, Daejeon 305-701, Korea. (Manuscript **Received** March 17, 2006; **Revised** July 14, 2006)

1.2 Descriptions of the nano-positioning system

Usually, nano-positioning systems adopt the flexure-guide which uses elastic deformations of material itself as guide mechanisms shown in Fig. 1. Flexure guides are free from wear and thus enable the positioning system to be controlled in nanometer level. (Lee et al., 2006a ; 2006b ; Banik et al., 2005) In this work, the simple linear parallel mechanism is used for educational purpose. PZT (Plumbum zirconate titanate) actuators are used as actuating sources for the nano-positioning system. The PZT actuator is capable of nanometer level positioning with a proper low-noise voltage amplifier and is very efficient actuating source because of a little power consumption. Even the PZT actuator suffer from a nonlinearity and accordingly hysteresis, the PZT actuator is widely used because of large holding force, fast response, vacuum-compatibility and long durability. As a feedback sensor, capacitive sensors having an ultimate resolution are used. Because this sensor is non-contact type, the moving body of the positioning system is not suffering from the sensor effect for example, mass loading which is inevitable in case of the accelerometers.

1.3 Descriptions of the training procedure of the education model of a nano-positioning system

The education model is comprised of two parts.

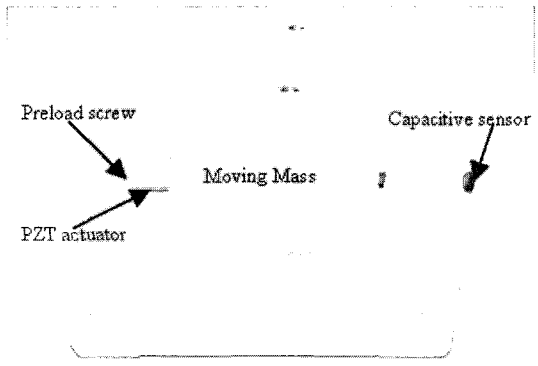

Fig. 1 Schema showing a nano-positioning system which use a flexure guide, a PZT actuator and a capacitive sensor

The first part is design procedures and second is experiments. In design part, the analytical method for finding the stiffness and the resonant frequency of the guide system is presented and the evidence is presented by using a commercial finite element analysis program. In experiments part, the experimental apparatus are described and the travel range, resonant frequencies, sine-tracking, multi-step responses (resolution) are investigated. The hysteresis and nonlinearity of the PZT actuator are measured. The feedback methodology accordingly, the comparison between an open and closed response are described. Moreover, the "separation frequency" which has newly been found in this work is described deeply. Finally, parasitic motion errors and the effect of external vibrations are dealt in this paper.

2. Design

2.1 Resonant frequency of the flexure guide

We used a simple notch-type linear spring as a flexure guide, as illustrated in Fig. 2, to investigate the large parasitic motion error. For the formulation of the equations of motion, kinetic energy, and potential energy of the four-bar linkage mechanism are derived, and then Lagrange's equation is used. This method is helpful for estimating the stiffness and the resonant frequency of the guide mechanism. (Kwon et al., 2003 ; Lee and Lee, 2005 ; Lee et al., 2005)

The kinetic energy of the four-bar linkage system of Fig. 2 is given as :

$$T=\frac{1}{2}M\dot{q}_1^2+2\times\frac{1}{2}m_l\left(\frac{\dot{q}_1}{2}\right)^2+2\times\frac{1}{2}I\left(\frac{\dot{q}_1}{L}\right)^2 \quad (1)$$

Here, M is the mass of moving body, m_l is the mass of the linkage (length : L) and I is the rotary inertia of the linkage. The potential energy is calculated using the angular deflection, as follows :

$$V=4\times\frac{1}{2}K_\theta\left(\frac{q_1}{L}\right)^2, \text{ while } \theta_z\cong\frac{q_1}{L} \quad (2)$$

Here, K_θ is the angular stiffness of the linkage. From Lagrange's equation, these two equations

are combined, as follows:

$$\frac{\partial}{\partial t}\left(\frac{\partial T}{\partial \dot{q}_1}\right)-\frac{\partial (T-V)}{\partial q_1}=F \tag{3}$$

Thus,

$$\left(M+\frac{1}{2}m_l+\frac{2}{L^2}I\right)\ddot{q}_1+\frac{4}{L^2}K_\theta q_1=F \tag{4}$$

From Eq. (4), the effective mass and the effective stiffness can be defined as follows:

$$M_{eff}=M+\frac{1}{2}m_l+\frac{2}{L^2}I,\ K_{eff}=\frac{4}{L^2}K_\theta \tag{5}$$

For the single-axis flexure hinge, application of moment M_z causes the flexure guide to deflect through angle θ_z about the z-axis as follows (Smith, 2000):

$$\frac{1}{K_\theta}=\frac{\theta_z}{M_z}=\frac{3}{2EbR^2}\left[\frac{1}{2\beta+\beta^2}\right]\cdot\left\{\left[\frac{1+\beta}{\gamma^2}+\frac{3+2\beta+\beta^3}{\gamma(2\beta+\beta^2)}\right]\cdot\left[\sqrt{1+(1+\beta-\gamma)^2}\right]+\left[\frac{6(1+\beta)}{(2\beta+\beta^2)^{3/2}}\right]\cdot\left[\tan^{-1}\left(\sqrt{\frac{2+\beta}{\beta}}\times\frac{(\gamma-\beta)}{\sqrt{1-(1+\beta-\gamma)^2}}\right)\right]\right\} \tag{6}$$

where t is notch hinge thickness, h is hinge width, b is hinge length, $\beta=t/2R$ and $\gamma=h/2R$. For the case of $\beta\ll 1$ and $\beta\ll\gamma$, Eq. (6) can be simplified as:

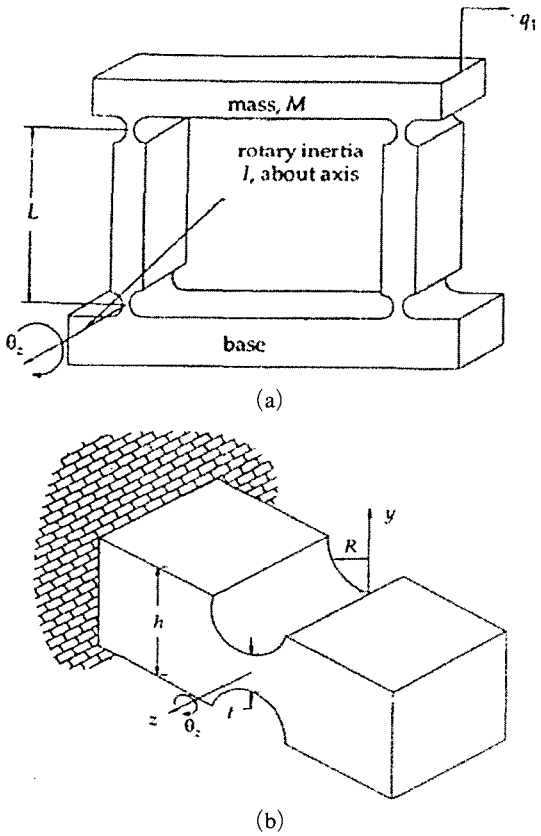

Fig. 2 Simple linear spring: (a) Notch type hinge and (b) Four-bar linkage type motion guide. (Smith, 2000)

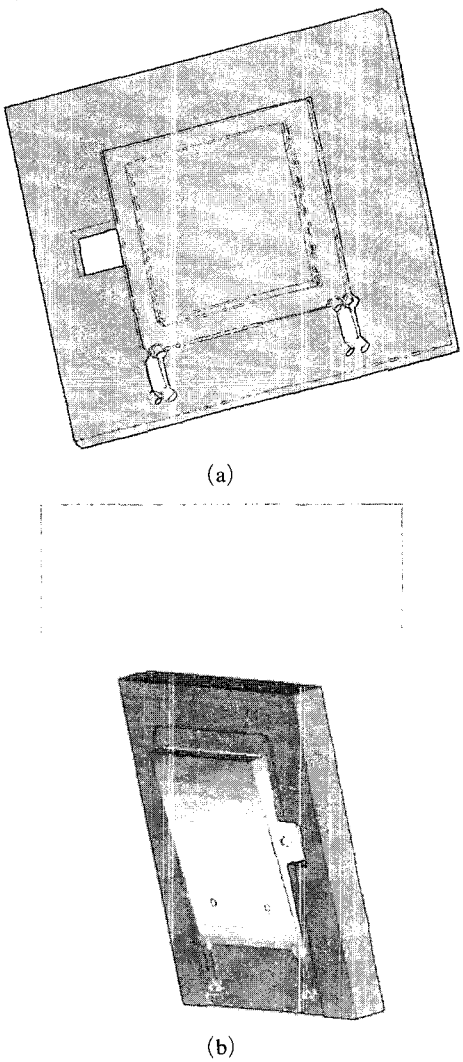

Fig. 3 (a) Resonant frequency: lateral direction (57.6 Hz), (b) Resonant frequency: vertical direction (174.9 Hz)

$$K_\theta=\frac{M_z}{\theta_z}=\frac{2Ebt^{5/2}}{9\pi R^{1/2}} \tag{7}$$

Thus,

$$K_{eff}=\frac{8Ebt^{5/2}}{9\pi L^2R^{1/2}} \tag{8}$$

The (original) resonant frequency of the flexure guide can be found from Eq. (9).

$$f_n=\frac{1}{2\pi}\sqrt{\frac{K_{eff}}{M_{eff}}} \tag{9}$$

Considering all the given dimensions and parameters (t=0.5, h=0.6, b=14, R=3 and L=20 (mm)), material: AL6061), the resonant frequency is calculated, as follows:

$$f_n=\frac{1}{2\pi}\sqrt{\frac{K_{eff}}{M_{eff}}}=56.9 \text{ Hz}$$

2.2 Finite element analysis of the resonant frequency

For the FEM analysis, we used a commercial program: ProMechanica™ (PTC corp.). The modeling was performed without considering the drive effect of the PZT actuator. Figure 3(a) shows the first lateral directional resonant frequency (57.6 Hz). The simulation result was in good agreement with the theoretical result.

3. Experiments

The objective of experiments is giving some insights on the nano-positioning system which comprise the PZT actuator, the simple linear guide, precision capacitive sensor and data acquisition systems. The open and closed loop step responses are measured to investigate the rising time, overshoot, settling time and the difference between feedback and no feedback. To investigate the tracking performances of the total system, the sine tracking responses are measured. As a check of the resolution of the total system, the multi-step response is measured. Finally, as a simple but educative application, the present nano-positioner is applied to a commercial atomic force microscope.

3.1 Experimental apparatus

The PZT actuator (AE0505D16) is a multilayered stacked type manufactured by NEC-Tokin Corp. The specifications of the PZT actuator are summarized in Table 1. The voltage amplifier for the PZT actuator is a MDT 694 of Thorlabs Corp. The specifications of the driver are summarized in Table 2. The data acquisition board is NI AT-MIO 16XE-50 (National Instrument Corp.) which can use Labview program. The specifications of the board are summarized in Table 3.

Table 1 Specifications of the PZT actuator

Displacement at 150V	17.4 (μm)
Generated force	850 (N)
Resonance frequency	69 (kHz)
Capacitance	1.4 (μF)
Size	5×5×20 (mm^3)

Table 2 Specifications of the PZT driver (MDT 694)

Output voltage range	0~150 (V)
3dB bandwidth	40 (kHz)
Output noise	1.5 (mVrms)
Max output current	60 (mA)
External input voltage range	0~10 (V)
External input gain	15 (V/V+/−5%)
Operating temperature	0~45 (℃)

Table 3 Specifications of the DAQ board

Sampling rate	20kS/s
A/D input	16bit 16CH
D/A output	12bit 2CH

Table 4 Driver of the capacitive sensor (DMT 22)

Bandwidth	20 (kHz)
Maximum error	0.3% F.S.
Maximum zero drift	0.02% F.S./℃
Output voltage	+/− 10 (VDC)
Operating temperature	4~50 (℃)
Operating range	10 (μm)
Sensitivity	2 (μm/V)
Resolution	1 (nm)

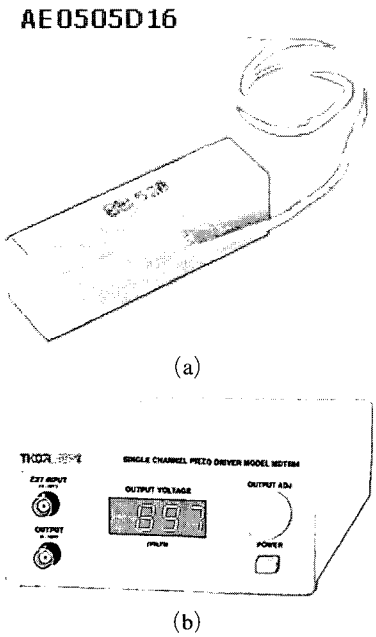

Fig. 4 (a) Multilayered PZT actuator (AE0505D16), (b) PZT driver (MDT 694)

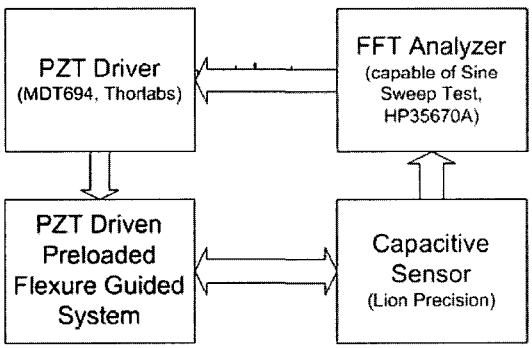

Fig. 5 Experimental setup

The driver of the capacitive sensor is DMT 22 of Lion precision corp. The specifications of the driver are summarized in Table 4. Total experimental setup is shown in Fig. 5. Here, a FFT analyzer is used to measure the resonant frequency of the nano-positioning system.

3.2 Open-loop test : Impulse response

To find resonant frequencies of the stage itself, the impulse responses are measured using dynamic signal analyzer. The higher resonance means the faster response which is useful in high-seed nano-positioning. The first resonant frequency is 54 Hz

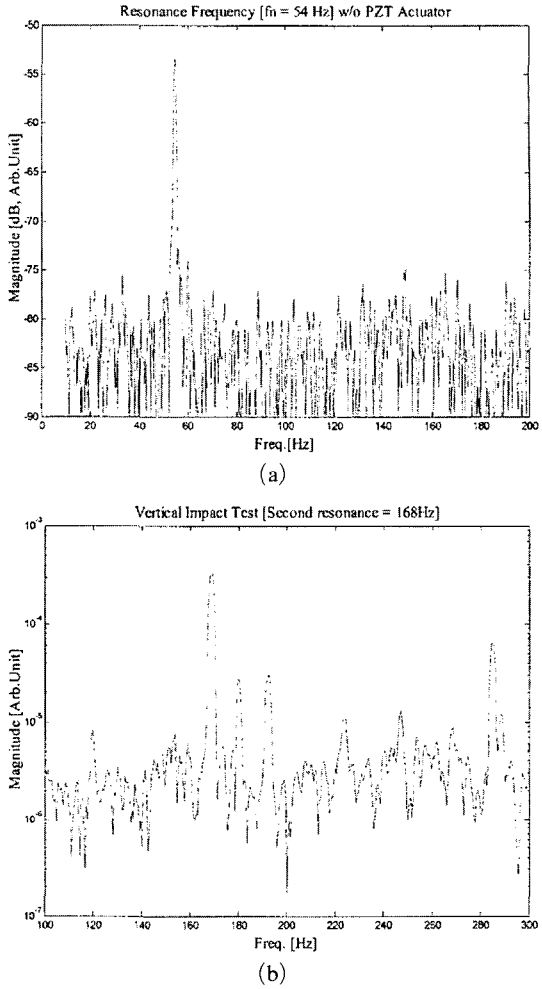

Fig. 6 Resonant frequencies : (a) lateral direction (54 Hz), (b) vertical direction (168 Hz)

in lateral direction and the second one is 168 Hz in vertical direction as in Fig. 6. From the results of Fig. 6, the similarity between analytic (57.6 Hz, 174.9 Hz) and experimental (54 Hz, 168 Hz) solutions is verified.

3.3 Open-loop test : Step response

In open-loop step response, we could observe the rising time, damping characteristics, stead-state error and creep phenomenon. Especially, the creep only occurs in open-loop operation, and can be eliminated by servo-control. Like hysteresis, creep is related to the effect of the applied voltage on the remanent polarization of the piezo-ceramics. Creep is the expression of the

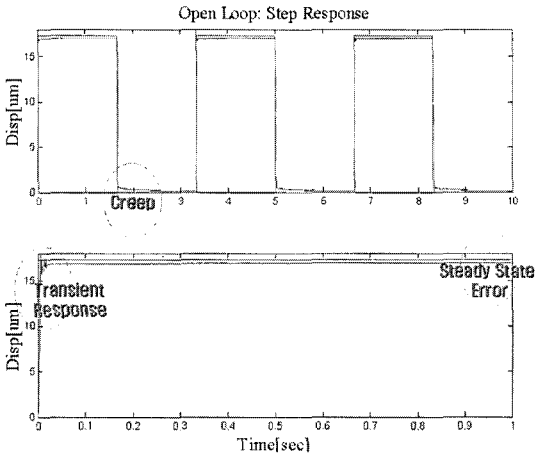

Fig. 7 Step response of the system in open-loop state. The creep phenomenon is clearly observed

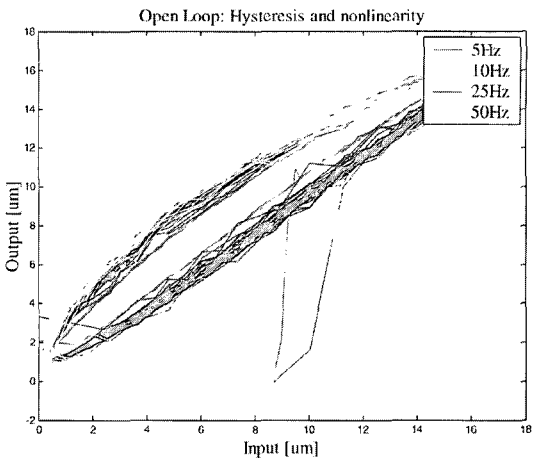

Fig. 8 Hysteresis and nonlinearity of the PZT actuator at various frequencies. As the input frequency increase, the magnitude of the hysteresis increase

slow realignment of the crystal domains in a constant electric field over time. If the operating voltage of a PZT is changed, after the voltage change is complete, the remanent polarization continues to change, manifesting itself in a slow creep. The rate of creep decreases logarithmically with time. As you can see from Fig. 7, the creep phenomenon is clearly observed. Moreover, the rising time is 5 ms, overshoot is 1 μm for 16 μm input, settling time is 50 ms, and the steady state error is 0.33 μm.

3.4 Open-loop test : Hysteresis

The absolute displacement generated by an open-loop PZT depends on the applied voltage and the piezo gain, which is related to the remanent polarization. Since the remanent polarization, and therefore the piezo gain, is affected by the electric field applied to the piezo, the deflection depends on whether the PZT was previously operated at a higher or a lower field strength. Hysteresis is typically on the order of 10% to 15% of the commanded motion. Hysteresis can be virtually eliminated in closed-loop PZT actuators. As you can see from Fig. 8, the hysteresis and nonlinearity are clearly observed and varied with input frequencies.

3.5 Open-loop test : Sine tracking

The sine tracking at open-loop state reveals the

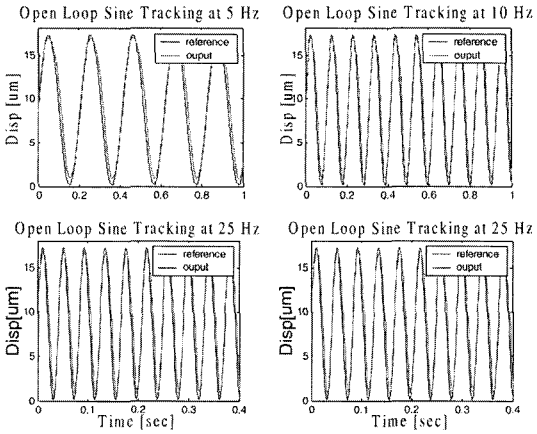

Fig. 9 Sine tracking of the system in open-loop state at various frequnencies

tracking capability of the system with respect to input. As you observe from Fig. 9, the peak difference between reference and output is increasing with higher input frequency which means decreasing controllability with higher speed.

3.6 Closed-loop test : Step response

To perform the closed-loop test, the setup is constructed as like Fig. 10. A gap sensor is used to measure the output of the stage, a DAG board (NI Corp.) is used to acquire data and a personal computer is used to control the system. The PID

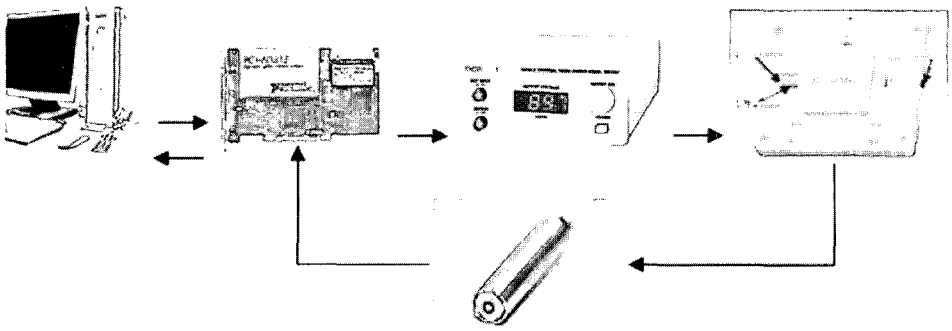

Fig. 10 Schema of the control system

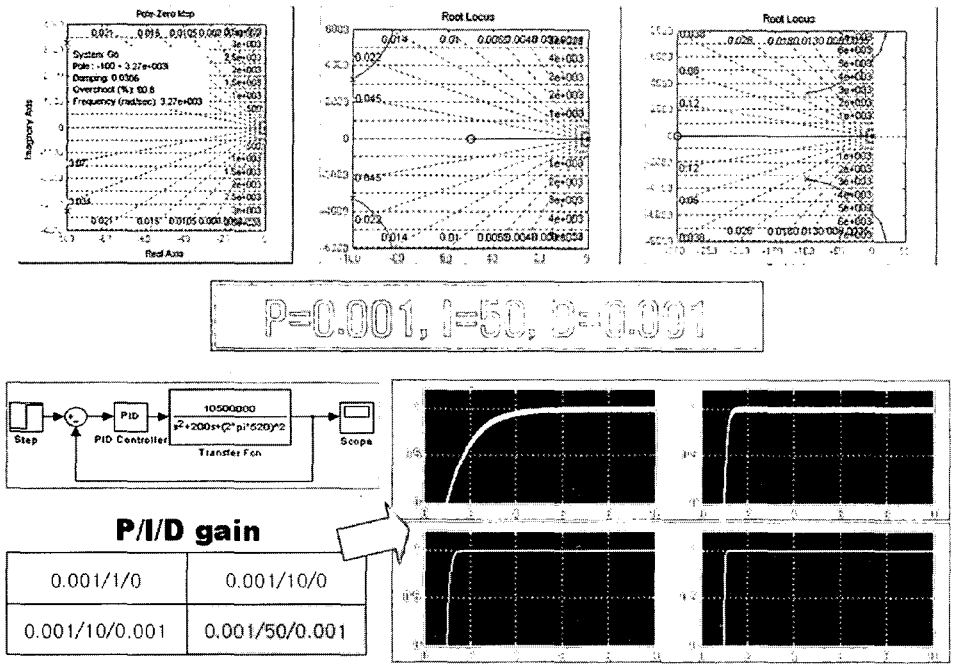

Fig. 11 Example of the PID gain tuning. The commercial MATLAB Simulink program was used

control scheme is used for simplicity but, the PID gains are optimized by using MATLAB Simulink. One example and procedure for the gain optimization is presented at Fig. 11. With the basis of the optimized PID gain, the closed-loop step response is performed as like Fig. 12. As you can observe from Fig. 12, the stage follows the step input faithfully and the transient response is improved comparing with the open-loop one.

3.7 Closed-loop test : Sine tracking

The closed-loop sine tracking is performed as like Fig. 13. As you can observe from Fig. 13, the stage follows the sine input faithfully comparing with the open-loop one.

3.8 Closed-loop test : Multi-step response

To access the system resolution in condition of the feedback, the multi-step test is performed as like Fig. 14. The system resolution is about 10 nm. Of course, the open-loop resolution is higher than the closed one because of no feedback. However, the resolution of the closed-loop is more important in real applications because the closed-loop resolution reflects the actual operating conditions.

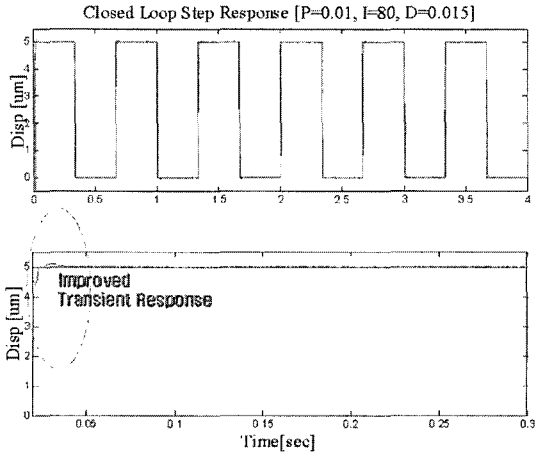

Fig. 12 Step response of the system in closed-loop state. The creep is eliminated by the feedback

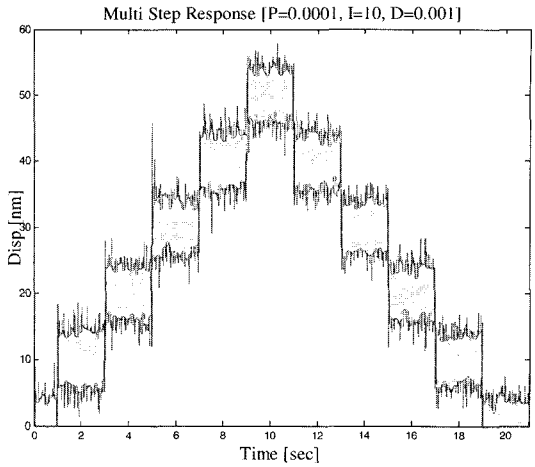

Fig. 14 Multi-step response showing the resolution of the total system including the feedback components

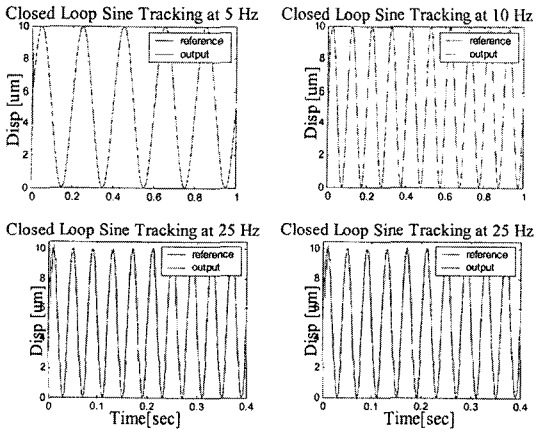

Fig. 13 Sine tracking of the system in closed-loop state at various frequencies

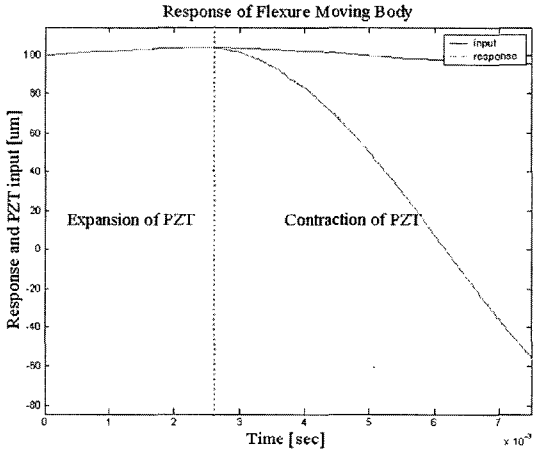

Fig. 15 Response of the moving body, explaining the separation frequency

3.9 Separation frequency

When the PZT actuator expands from a rest position at any given frequency, the moving body of the flexure guide will follow the PZT input motion due to a high actuation force, as illustrated in Fig. 15, which results in the positioning system acting as a single body. However, when the PZT actuator contracts at t_0 (Fig. 15), the moving body may or may not follow the PZT actuator, depending on the acceleration level of the moving body at t_0. This may cause physical separation between the PZT and the moving body. If we consider that a preload (A_0) and a driving input $(A_i \cos(\omega_d t))$ are applied to the flexure guide, then the combined input to the flexure guide is $x_i = A_0 + A_i \cos(2\pi f_d t)$. The preload is given via the preloading screw during assembling, and the driving input is given via the PZT actuator. When the flexure system is assumed to be a lightly-damped 2nd-order system, the output displacement will be $x_o = (A_0 + A_i) e^{-\zeta 2\pi f_n t} \cos(2\pi f_n t)$, where ζ is the damping ratio and f_d is the driving frequency. If we assume no damping in the flexure system, the output displacement will be $x_o = (A_0 + A_i) \cos(2\pi f_n t)$, which indicates free

vibration with an initial displacement (A0+Ai), as illustrated in Fig. 15. In our system, the PZT actuator is attached to a flexure's moving body by using a preloading screw without any adhesive bonding. Therefore, separation can occur.(Lee and Gweon, 2006)

The condition for the moving body of the flexure guide to follow the driving input is that the acceleration of the moving body, $a_o(t)$, should be greater than or equal to the acceleration of the driving input, $a_i(t)$, applied on the PZT. Otherwise, the PZT will contract faster than the recovering rate of the flexure moving body, resulting in separation of the PZT from the flexure guide. To determine the frequency at which separation occurs between the flexure guide and the PZT actuator, we can use the following condition at initial time t_0:

$$a_o(t_o) \leq a_i(t_o) \tag{10}$$

Here, $a_i(t) = -A_i 2\pi f_d^2 \cos(2\pi f_d t)$ represents the acceleration of the PZT actuator during contraction, and $a_o(t) = -(A_o + A_i) 2\pi f_n^2 \cos(2\pi f_n t)$ represents the acceleration of the flexure moving body during the PZT contraction. The frequency at which separation occurs is defined as the separation frequency. At the separation frequency (f_s),

$$|a_o(t_o)| = |a_i(t_o)| \tag{11}$$

$$\begin{aligned} &\Rightarrow (A_o + A_i) f_n^2 = A_i f_s^2, \text{ where } f_d = f_s \\ &\Rightarrow f_s = \left(\sqrt{\frac{A_o + A_i}{A_i}}\right) f_n \\ &\Rightarrow f_s = (\sqrt{d+1}) f_n, \text{ where } d = \frac{A_o}{A_i}, \text{ and} \\ &\frac{f_s}{f_n} = \sqrt{d+1} \end{aligned} \tag{12}$$

As can be seen from Eq. (12), the separation frequency depends on the preload (A_0), the driving input amplitude (A_i), and the original resonant frequency of the flexure guide (f_n). Here, the normalized preload (d) is defined as the ratio of the preload to the input amplitude. If $f_d \leq f_s$, then $a_o(t_0) \geq a_i(t_0)$, which means that the moving body will follow the PZT motion as one body during both the expansion and the contraction of the PZT. However, if $f_d > f_s$, then $a_o(t_0) < a_i(t_0)$, which means the moving body will tend to return to its rest position at a slower rate than the PZT contraction speed. This means that separation between the PZT actuator and the moving body will occur. After finishing its contraction, the PZT actuator starts to expand with its driving frequency. However, the moving body of the flexure guide is still contracting. Accordingly, a pseudo-resonant shock will occur between the PZT actuator and the moving guide when they meet. Moreover, we cannot control the flexure system at this higher driving input frequency. These are the main reasons for the separation frequency, which is the point of the present study. The lower limit of the separation frequency is the resonant frequency of the original flexure-guide system without the preload. The upper limit of the separation frequency is apparently $f_s^u = ((K_{eff} + K_p)/M_{eff})^{1/2}$. Here, K_p is the stiffness of the PZT actuator. When considering the upper limit of the separation frequency, the PZT stiffness is just added to the flexure guide stiffness, assuming that the PZT is bonded to the flexure's moving body with a strong adhesive material.

To find the separation frequency at various preload conditions and input amplitudes, we adopted the sine-sweep test. During the sine-sweep test at a given preload and given input amplitude, the input voltage to the PZT driver was constant, and the driving frequency was varied within a certain frequency range. Simultaneously, we measured the displacement of the flexure's moving body by using a gap sensor. Then, we plotted the magnitude and the phase of the output/input.

The experiments were performed at various preloading conditions and input amplitudes to find the separation frequency (f_s). Figure 16 shows that $f_s = 510$ Hz for a preload of 300 μm and a input amplitude of 3.88 μm. Here, the normalized preload (d) is about 77.3. From DC to the separation frequency, the magnitude of the response is nearly equal to the input amplitude. However, near the separation frequency, the response shows a resonance-like peak, though it is not an actual resonance, and the phase changes abruptly. These

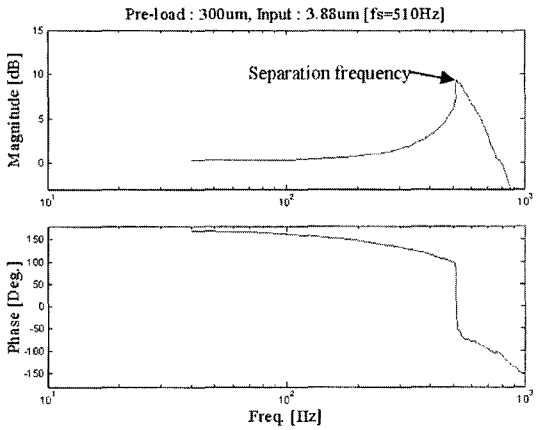

Fig. 16 Response/input relation for a preload of 300 μm and an input amplitude of 3.88 μm

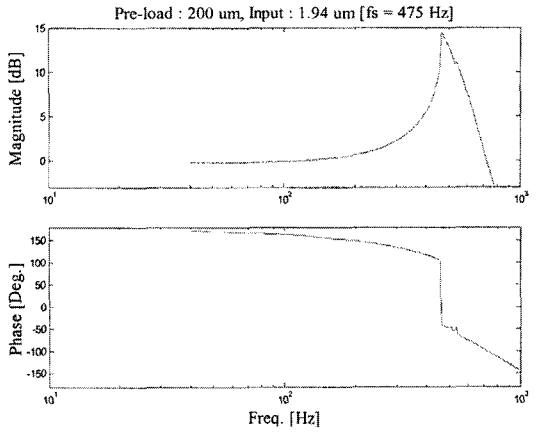

Fig. 18 Response/input relation for a preload of 200 μm and an input amplitude of 1.94 μm

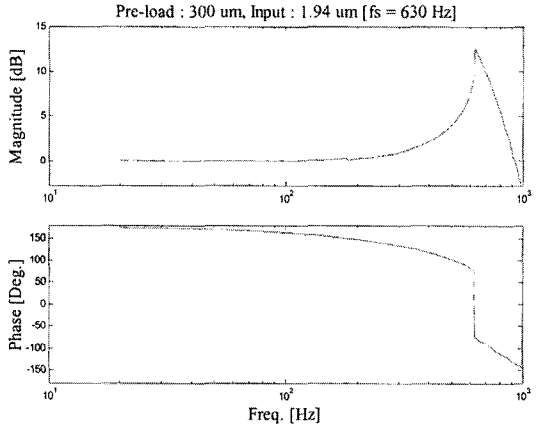

Fig. 17 Response/input relation for a preload of 300 μm and an input amplitude of 1.94 μm

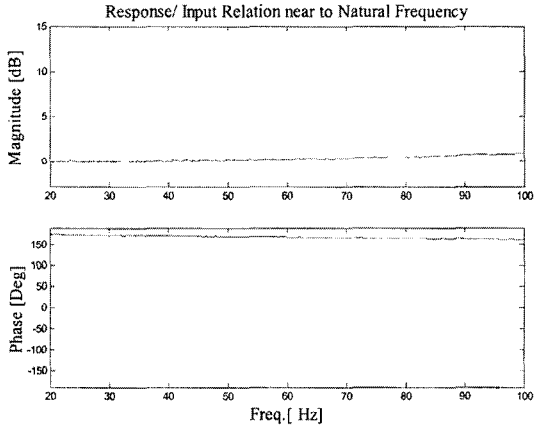

Fig. 19 Response/input relation near the original resonant frequency (54 Hz)

are the typical characteristics of the separation behavior and were proven experimentally.

Figure 17 shows that f_s=630 Hz for a preload of 300 μm and an input amplitude of 1.94 μm (d=154.6). In this test, the input amplitude was down to half that for the case shown in Fig. 16, but the preload was unchanged. The result showed that the separation frequency is inversely proportional to the input amplitude, as in Eq. (12). The response pattern is that same as that shown in Fig. 17, but the separation frequency is higher.

Figure 18 shows that f_s=475 Hz for a preload of 200 μm and an input amplitude of 1.94 μm (d=103.1). In this test, the preload is decreased, but the input amplitude is the same as that shown in Fig. 17. This result shows that the separation frequency is proportional to the preload, as in Eq. (12).

For clarity, we performed a band-limited sine-sweep test that focused on the original resonant frequency (Fig. 19). The preload and the input are the same as those of the case shown in Fig. 17. The result shown in Fig. 19 demonstrates that when the PZT actuator is assembled into the flexure system with an appropriate preload, there is no resonant response near the original resonant frequency of the flexure system. This means that we can operate the preloaded flexure system at a higher frequency than the original resonant fre-

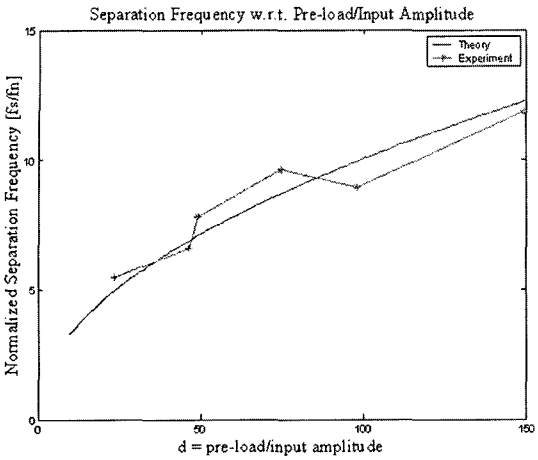

Fig. 20 Dependency of the separation frequency on the preload/input amplitude

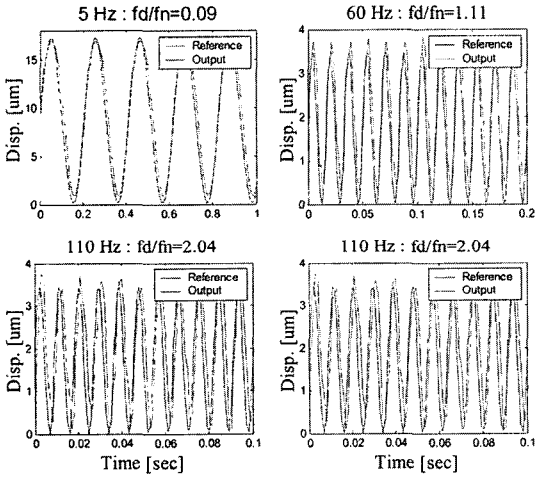

Fig. 21 Open-loop sine-tracking response : the original resonant frequency (fn) =54 Hz, the separation frequency (fs) =416 Hz, the driving frequency (fd) =5~130 Hz, the preload= 200 μm and the input amplitude=3.88 μm (d=51.5)

quency of the flexure itself.

The theoretical results (Eq. (12)) were compared with experimental results, as shown in Fig. 20. The graph shown in Fig. 20 demonstrates that the separation frequency is proportional to the normalized preload. The error between the theory and the experiment is less than 10%. This proves our theory that the separation frequency depends largely on the selection of the preload, and on the input amplitude of the PZT. The lower limit of the separation frequency will be the original resonant frequency of the moving mass. If we increase the ratio of the preload to the input amplitude, then the separation frequency will approach to $f_s^6=((K_{eff}+K_p)/M_{eff})^{1/2}$, which represents the upper limit of the separation frequency.

Open-loop sine-tracking experiments were performed to validate the concept of the separation frequency and to check the system's response at a frequency higher than the original resonant frequency (54 Hz). The results shown in Fig. 21 reveal that up to 130 Hz, the moving body of the flexure system follows the PZT actuator well. Without considering the preload effect on the response of the flexure system, one may think that the maximum driving frequency is determined by the original resonant frequency of the flexure system. However, the experimental and the theoretical results of the present study show that the maximum driving frequency is determined by the separation frequency, which depends on both the ratio of the preload to the input amplitude and the original resonant frequency.

3.10 Application : Atomic force microscope

The nano-positioning device of the present study uses a PZT actuator and a flexural guide. These kinds of the devices are used as sample scanners for atomic force microscopes (UME and Timmerman 1995). To prove the capability for nanometer-level resolution, we measured the resolution using a multi-step response (Rizzoni and Keyhani, 1995). Figure 14 shows that the resolution was less than 10 nm. Moreover, a real AFM image was acquired by using the commercial AFM head (XE-150, www.psia.co.kr). The present device is just a one-axis positioner, which means that a single line profile could be acquired by the AFM, as like Fig. 22(a). As Fig. 22(a) shows, the line profile represents the pitch of the standard grating of Fig. 22(b). Even though this rather simple type of positioner has not been used in real applications, we can get insight into a nano-positioning device and use the idea of the separation frequency to increase the system bandwidth.

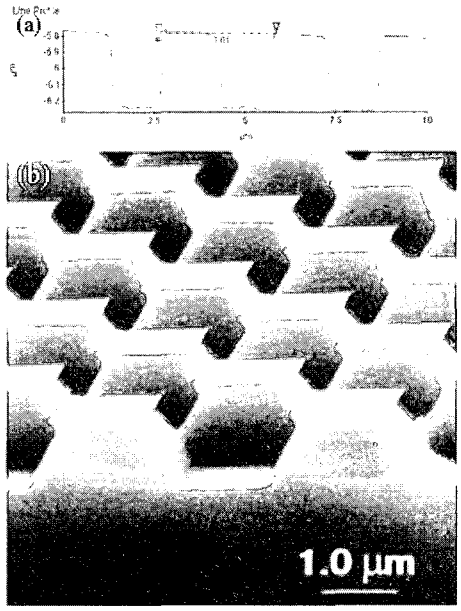

Fig. 22 (a) Line profile of the standard grating (TGX1 (www.ntmdt.com) with a 3 μm pitch) and (b) SEM image of the standard grating (TGX1)

4. Conclusion and Discussions

As a "role-model" of the nano-positioning training for practicing nano-engineers, the education model of KAIST is presented in this article. The method of finding the stiffness and resonant frequency which meet the system specifications is proposed. Also, the various experimental method are presented to access the performance of the designed stage, for example, step response, sine-tracking and multi-step response of both case of open and closed loop control. Moreover, the creep, nonlinearity and hysteresis of the PZT actuator are clearly observed via the experiments. Finally, the concept of the "separation frequency" is described and verified by experiments. The separation frequency is proportional to the ratio of the preload to the driving input amplitude. The maximum driving frequency is determined by the separation frequency, not by the original resonant frequency. If it is difficult to increase the original natural frequency due to design constraints, then we can use the dependency of the separation frequency on the normalized preload. A larger preload will result in a higher separation frequency and, accordingly, a higher maximum driving frequency without any change in the original natural frequency.

In designing the nano-positioner, the machining tolerance should be considered. To give some insight on the machining tolerance, we explain a following example. The thickness of current nano-positioner is 0.5 mm. If the machining tolerance is ± 20 μm, then the natural frequency will changed by 5 Hz. This large change is about 10% change comparing with the original resonant frequency.

Because the guide of the current research is a simple linear spring type, there should be large parasitic motion (unwanted crosstalk between axes). To access the parasitic motion, the y motion is measured when the guide is moving along x-direction as like Fig. 23. The input amplitude of x-direction is 10 μmp-p, the parasitic motion of y-axis is about 0.15 μmp-p about 1.5% of input of x-direction. To be a good guide for the nano-positioner, this large parasitic motion should be eliminated. To do so, a sure method is to use a double compound mechanism.

The floor vibration is important for clean data and control of the nano-positioner. To get insight of the floor vibration level, the actual floor and air table vibration are measured and compared as like Fig. 24 in usual operating laboratory condition at early morning time. The measured data are along the vertical direction. As you can see from the data of Fig. 24, the usual floor vibration level is less than 10^{-4} g, and the air table vibration after vibration suppression is less than 10^{-5} g. Even this small vibration could affect the performance of the nano-positioner as shown in Fig. 25. From Fig. 25, the system resolution is deteriorated with no vibration suppression system. Usually, because the passive type of vibration isolator has its own resonant frequency (a few Hz, Fig. 23), the active vibration isolator is suggested for the low frequency application.

For a final discussion, the thermal effect is important for the long-term usage of the nano-positioner. Usually, materials expand or contract with temperature variation. As one measure of

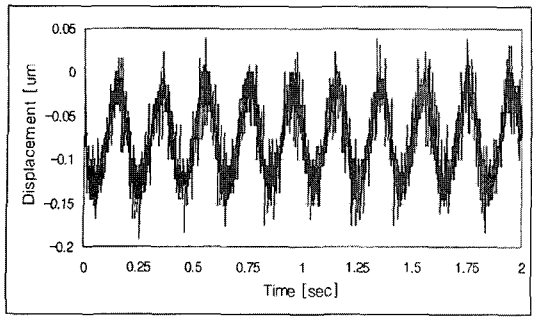

(a)

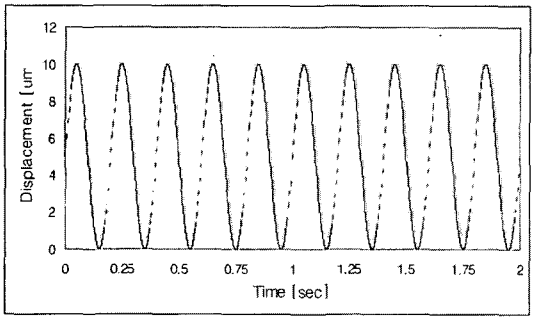

(b)

Fig. 23 (a) Response of the system along x-axis, (b) Parasitic motion of the y-axis caused by the guide

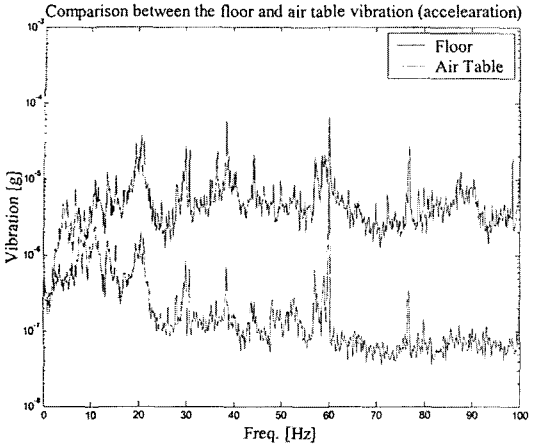

Fig. 24 Comparison between the floor and the air table vibration. Approximately, one order of the floor vibration is decreased by the passive air table

the thermal effect, the drift of the capacitive sensor was measured during 160 minutes as like Fig. 26. Typically, the thermal drift is slowly varying with

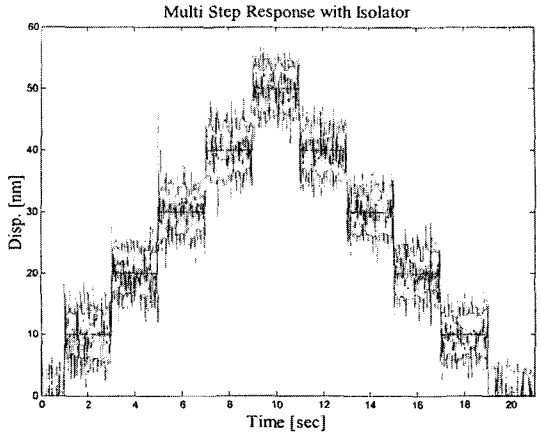

(a)

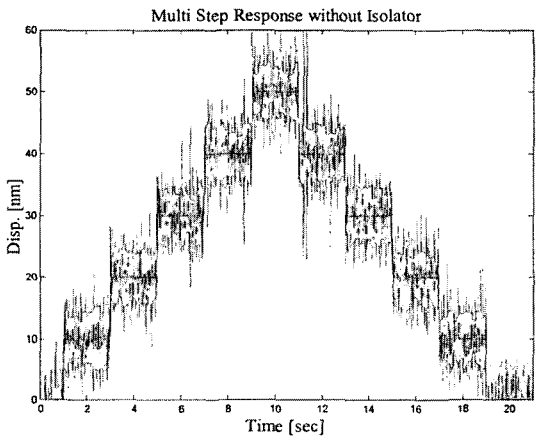

(b)

Fig. 25 Influence of the floor vibration. The system resolution is deteriorated by the external floor vibration

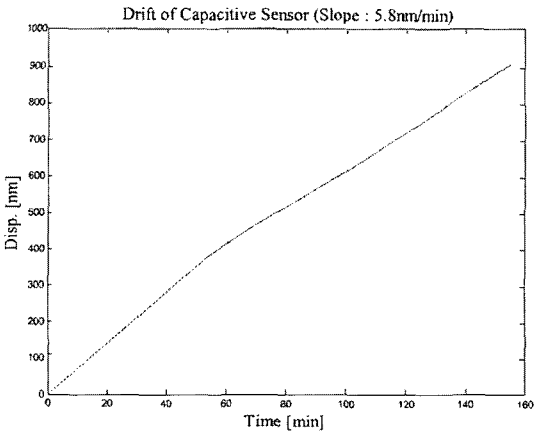

Fig. 26 Drift of the capacitive sensor. The slop of the drift is 5.8 nm/min

time. The slope of the thermal drift of Fig. 26 is 5.8 nm/min.

References

Acar, M. and Parkin, R. M., 1996, "Engineering Education for Mechatronics," *IEEE Transactions on Industrial Electronics*, Vol. 43, No. 1, pp. 106~112.

Banik, R., Lee, D. Y. and Gweon, D. G., 2005, "A High-speed Miniature Screening Gaschromatograph with Flame Ionization Detector," *Journal of Mechanical Science and Technology*, Vol. 19, No. 12, pp. 2197~2204.

Bojarski, Z., Hetmariczyk, M., Jeziorski, L., Morawiec, H., Slusarski, L. and Wojciechowski, St., 1995, "Material Science and Engineering Education in Poland," *Materials Science and Engineering A*, Vol. 199, pp. 27~34.

Chisholm, A. W. J., 1990, "An Engineering Design Analogy for Engineering Education," *Computers in Industry*, Vol. 14, pp. 197~204.

Fraser, C. J., Milne, J. S. and Logan, G. M., 1992, "An Educational Perspective on Applied Mechatronics," *Mechatronics*, Vol. 3, No. 1, pp. 49~57.

Giurgiutiu, V., Lyons, J., Rocheleau, D. and Liu, W., 2005, "Mechatronics/Microcontroller Education for Mechanical Engineering Students at the University of South Carolina," *Mechatronics*, Vol. 15, pp. 1025~1036.

Kwon, J., Hong, J., Kim, Y. S., Lee, D. Y., Lee, S. M. and Park, S. I., 2003, "Atomic force Microscope with Improved Scan Accuracy, Scan Speed and Optical Vision," *Review of Scientific Instruments*, Vol. 74, No. 10, pp. 4378~4383.

Lee, D. Y. and Lee, M. Y., 2005, "A Flexure Guided Planar Scanner for Scanning Probe Microscope; Part 1: Design and Analysis of Static and Dynamic Properties," *Trans. of the KSNVE*, Vol. 15, No. 6, pp. 667~673.

Lee, D. Y. and Gweon, D. G., 2006, "Pseudo-Resonant Effect on a Flexure-Guided Nano-Positioning System," *Journal of the Korean Physical Society*, Vol. 48, No. 3, pp. 363~370.

Lee, D. Y., Kim, D. M. and Gweon, D. G., 2006a, "Design and Evaluation of Two Dimensional Metrological Atomic Force Microscope using a Planar Nanoscanner," *Japanese Journal of Applied Physics*, Vol. 45, No. 3B, pp. 2124~2127.

Lee, D. Y., Lee, M. Y. and Gweon, D. G., 2006b, "Orthogonality Correction of Planar Sample Scanner for Atomic Force Microscope," *Japanese Journal of Applied Physics*, Vol. 45, No. 13, pp. L370~L372.

Lee, D. Y., Lee, M. Y. and Gweon, D. G., 2005, "A Flexure Guided Planar Scanner for Scanning Probe Microscope; Part 2: Evaluation of Static and Dynamic Properties," *Trans. of the KSNVE*, Vol. 15, No. 11, pp. 1295~1302.

Meek, S., Field, S. and Devasia, S., 2003, "Mechatronics education in the Department of Mechanical Engineering at the University of Utah," *Mechatronics*, Vol. 13, pp. 1~13.

Rizzoni, G. and Keyhani, A., 1995, "Design of Mechatronic Systems: an Integrated Inter-departmental Curriculum," *Mechatronics*, Vol. 5, No. 7, pp. 845~853.

Smith, S. T., 2000, "Flexures: Elements of Elastic Mechanisms," *Gordon and Breach Science Publishers*, pp. 180.

Tan, K. K., Lee, T. H., Dou, H. F. and Lim, S. Y., 1998, "Various Developments in Mechatronics in Asia," *Mechatronics*, Vol. 8, pp. 777~791.

UME, C. and Timmerman, M., 1995, "Mechatronics Instruction in the Mechanical Engineering Curriculum at Georgia Tech," *Mechatronics*, Vol. 5, No. 7, pp. 723~741.

Ye, X., Peng, W., Chen, Z. and Cai, Y. Y., 2004, "Today's Students, Tomorrow's Engineers: an Industrial Perspective on CAD Education," *Computer-Aided Design*, Vol. 36, pp. 1451~1460.